Enhanced pyroelectric response from domain-engineered lead-free (K_{0.5}Bi_{0.5}TiO₃-BaTiO₃)-Na_{0.5}Bi_{0.5}TiO₃ ferroelectric ceramics

Atul Thakre^{1,+}, Deepam Maurya^{3,+}, Do Yoen Kim¹, Yunseok Kim⁴, Panithan Sriboriboon⁴,

Il-Ryeol Yoo⁵, Shashank Priya⁷, Kyung-Hoon Cho^{5,*}, Hyun-Cheol Song^{6,*} and Jungho Ryu^{1,2,*}

¹School of Materials Science and Engineering, Yeungnam University, Gyeongsan, Gyeongbuk 38541, Korea

²Institute of Materials Technology, Yeungnam University, Gyeongsan, Gyeongbuk 38541, Korea ³Center for Energy Harvesting Materials and Systems (CEHMS), Virginia Tech, 310 Durham Hall, Blacksburg, VA 24061, USA

⁴School of Advanced Materials Science and Engineering, Sungkyunkwan University (SKKU), Suwon, Gyeonggi-do 16419, Korea

⁵School of Materials Science and Engineering, Kumoh National Institute of Technology, Gumi, Gyeongbuk 39177, Korea

⁶Center for Electronic Materials, Korea Institute of Science and Technology (KIST), Seoul, 02792, Korea 39177, Republic of Korea

⁷Materials Research Institute, Pennsylvania State University, PA 16801, USA

⁺ These authors contributed equally to this work.

Corresponding Authors:

Jungho Ryu

School of Materials Science and Engineering, Yeungnam University, Gyeongsan, Gyeongbuk

38541, Korea

Institute of Materials Technology, Yeungnam University, Gyeongsan, Gyeongbuk 38541, Korea

E-mail: jhryu@ynu.ac.kr

Hyun-Cheol Song

Center for Electronic Materials, Korea Institute of Science and Technology (KIST), Seoul,

02792. Korea

E-mail: hcsong@kist.re.kr

Prof. K. H. Cho

School of Materials Science and Engineering, Kumoh National Institute of Technology, Gumi,

Gyeongbuk 39177, Korea

E-mail: khcho@kumoh.ac.kr

Abstract

Enhanced pyroelectric response is achieved via domain engineering from [001] grain-oriented,

tetragonal-phase, lead-free 0.2(2/3K_{0.5}Bi_{0.5}TiO₃-1/3BaTiO₃)-0.8Na_{0.5}Bi_{0.5}TiO₃ (KBT-BT-NBT)

ceramics prepared by a templated grain growth method. The [001] crystallographic orientation

leads to large polarization in tetragonal symmetry; therefore, texturing along this direction is

employed to enhance the pyroelectricity. X-ray diffraction analysis revealed a Lotgering factor

(degree of texturing) of 93 % along the [001] crystallographic direction. The textured KBT-BT-

NBT lead-free ceramics showed comparable pyroelectric figures of merit to those of lead-based

ferroelectric materials at room temperature (RT). In addition to the enhanced pyroelectric response

at RT, an enormous enhancement in the pyroelectric response (from 1750 to 90900 µC m⁻² K⁻¹)

was achieved at the depolarization temperature because of the sharp ferroelectric to

antiferroelectric phase transition owing to coherent 180° domain switching. These results will

2

motivate the development of a wide range of lead-free pyroelectric devices, such as thermal sensors and infra-red detectors.

Keywords: pyroelectric, lead-free material, texturing, template grain growth, ferroelectric phase transition

1. Introduction

Pyroelectric materials exhibit a spontaneous change in polarization when subjected to temperature fluctuations. Such a response to temperature fluctuations results in accumulated charge carriers at the electrodes due to a net change in polarization. Pyroelectric materials have excellent potential applicability in high-sensitivity thermal sensors, imaging devices like bolometers, and thermal energy harvesters. The figure of merit (FoM) values of the pyroelectric materials in these applications depend primarily on their high pyroelectric coefficient. In the past few decades, lead-based ferroelectric (FE) ceramics such as lead zirconate titanate (PZT) and its derivatives have been widely studied and utilised in these applications owing to their excellent pyroelectric performance. However, the fabrication and disposal of lead-based materials and devices at an industrial scale lead to environmental and atmospheric issues owing to the difficulty of removing lead during the recycling of the components [1,2]. The toxicity of lead has driven the research community to develop lead-free alternatives to lead-based piezoelectric ceramics. Although the piezoelectric properties of lead-free ceramics are inferior to those of their lead-based counterparts, recent studies have shown that the pyroelectric properties of both are on par [3–6]. Various alternative material forms such as single crystals have been studied to achieve better pyroelectric response from lead-free materials than from lead-based ceramics [4,7,8]. Several leadfree piezoelectric and pyroelectric compositions and their modified forms have been reported, including $K_{1-x}Na_xNbO_3$ (KNN), $Bi_{0.5}Na_{0.5}TiO_3$ (BNT), $Sr_{0.5}Ba_{0.5}Nb_2O_6$ (SBN), and (1– x)Ba(Zr_{0.2}Ti_{0.8})O₃-x(Ba_{0.7}Ca_{0.3})TiO₃ (BZT-BCT) [9–13]. Most of these lead-free materials have some limitations; for example, KNN-based ceramics are sensitive to moisture and are difficult to sinter because of the presence of volatile alkali elements [14]. BZT-BCT-based ceramics have shown excellent piezoelectric properties at room temperature; however, their low Curie

temperature (T_c < 93 °C) presents a challenge [15,16]. Meanwhile, K_{0.5}Bi_{0.5}TiO₃-BaTiO₃-Na_{0.5}Bi_{0.5}TiO₃ (KBT-BT-NBT)-based perovskites are promising for both piezoelectric and pyroelectric applications owing to their excellent field-dependent response and high depolarization temperature. Compositions near the morphotropic phase boundaries of this system exhibit large remanent polarization (~24 μ C/cm²) and high T_c (~280 °C).

The FE phase of the Na_{0.5}Bi_{0.5}TiO₃-BaTiO₃ (NBT-BT)-based FE materials has been found to exhibit sharp changes in FE polarization in the vicinity of transition temperatures. This system exhibits several phase transitions: FE to antiferroelectric (AFE) or relaxor FE (RFE) phase transition at the depolarization temperature ($T_d \approx 100$ to 165 °C) and AFE to paraelectric phase transition in the range of 225–292 °C either at T_c or at the maximum dielectric permittivity temperature (T_m) [17]. Phase transitions can strongly influence the piezoelectric/FE and pyroelectric responses. The FE phase transitions between the polar and nonpolar states cause a large gradient in electrical polarization, which amplifies the pyroelectric response [18,19].

The degree of the pyroelectric effect in any material is determined by its pyroelectric coefficient (p). The p is defined as the change in the spontaneous polarization when the material is heated (or cooled) at a uniform rate, and can be expressed as,

$$p = \frac{dP}{dT} = \frac{1}{A}\frac{dQ}{dT} = \frac{1}{A}\frac{dQ}{dt}\frac{dt}{dT} = \frac{1}{A}I\frac{dt}{dT},\tag{1}$$

where P is the spontaneous polarization, T is the temperature, Q is the induced charge at the electrode, A is the surface area of the electrode, and I is the pyroelectric current. The dt/dT is the inverse of the heating rate. As reported earlier, the pyroelectric effect is maximised during phase transitions [4]. The enhancement in the p of ceramics can be achieved in various ways such as (a)

the microstructural engineering of the ceramics, (b) alteration of the position of the composition in the vicinity of the morphotropic phase boundary and thereby symmetry, and (c) defect engineering of the ceramic composition. Several attempts have been made to achieve a maximum pyroelectric response through the modulation of phase transitions in FE materials via dopant engineering and the synthesis of ternary solid solutions based on the NBT-BT base composition [8,20,21]. However, the doping of lead-free FE materials has been found to alter the temperature dependence of the polarization owing to the shift in the AFE-FE phase transition temperature (T_d). A decrease in T_d is detrimental to many piezoelectric and FE applications.

Enhanced FE/piezoelectric properties can be achieved in crystallographically textured FE ceramics (through microstructural engineering) [22–24]. [001]-textured tetragonal FE ceramics show a large polarization along the textured direction, which is also the spontaneous polarization direction for tetragonal FE materials. The intrinsic spontaneous polarization, P_s , along the polar axis of the mono domain crystal for the tetragonal phase is given by the relationship, $P_{s,<001>}=(3)^{1/2}$ $P_{s,<111>}$ [25]. The polarization magnitude of random polycrystalline ceramics is between those of <001> and <111> textured ceramics owing to the averaging of the magnitude in the three-dimensional space. Texturing of the FE ceramic further facilitates polarization switching under an applied field or stress [26]. Thus, textured FE ceramics can show a higher pyroelectric response owing to the enhanced polarization and temperature gradient of polarization. In addition, significant decreases in the dielectric constant (ε_r) and loss tangent ($\tan \delta$) greatly enhance the corresponding FoM values [27]. Moreover, the phase changes near T_d can play an important role in determining the pyroelectric characteristics. However, fundamental mechanisms governing the FE/ferroelastic transitions in the KBT-NBT-BT system are not fully understood [28,29].

The overarching goal of this study is to achieve an enhanced pyroelectric response from lead-free textured materials, as schematically illustrated in **Fig. 1a**. Here, we report the enhanced pyroelectric response of textured KBT-BT-NBT ceramics synthesised via a templated grain growth (TGG) method. A schematic of the synthesis process is shown in **Fig. 1b**. We obtained significant enhancements in the FoM values (from current responsivity (F_i), voltage responsivity (F_v), and detectivity (F_D) of 0.92×10^{-10} mV⁻¹, 0.015 m² C⁻¹, and 0.53×10^{-5} Pa^{-1/2}, respectively, to F_i , F_v , and F_D of 0.92×10^{-10} mV⁻¹, 0.035 m² C⁻¹, and 0.53×10^{-5} Pa^{-1/2}) at room temperature and 100 Hz. Moreover, the coefficient calculated from the measured thermally stimulated depolarization current (TSDC) density, p_{TSDC} , is 326 μ C m⁻² K⁻¹ at room temperature (RT); however, a remarkable p_{TSDC} value of 90900 μ C m⁻² K⁻¹ was obtained at T_d . The dielectric and FE properties and domain structures were investigated to understand the relationship between the phase transition behaviour and pyroelectricity. Finally, we delineate the fundamental reasons for the giant pyroelectric response of textured KBT-BT-NBT ceramics.

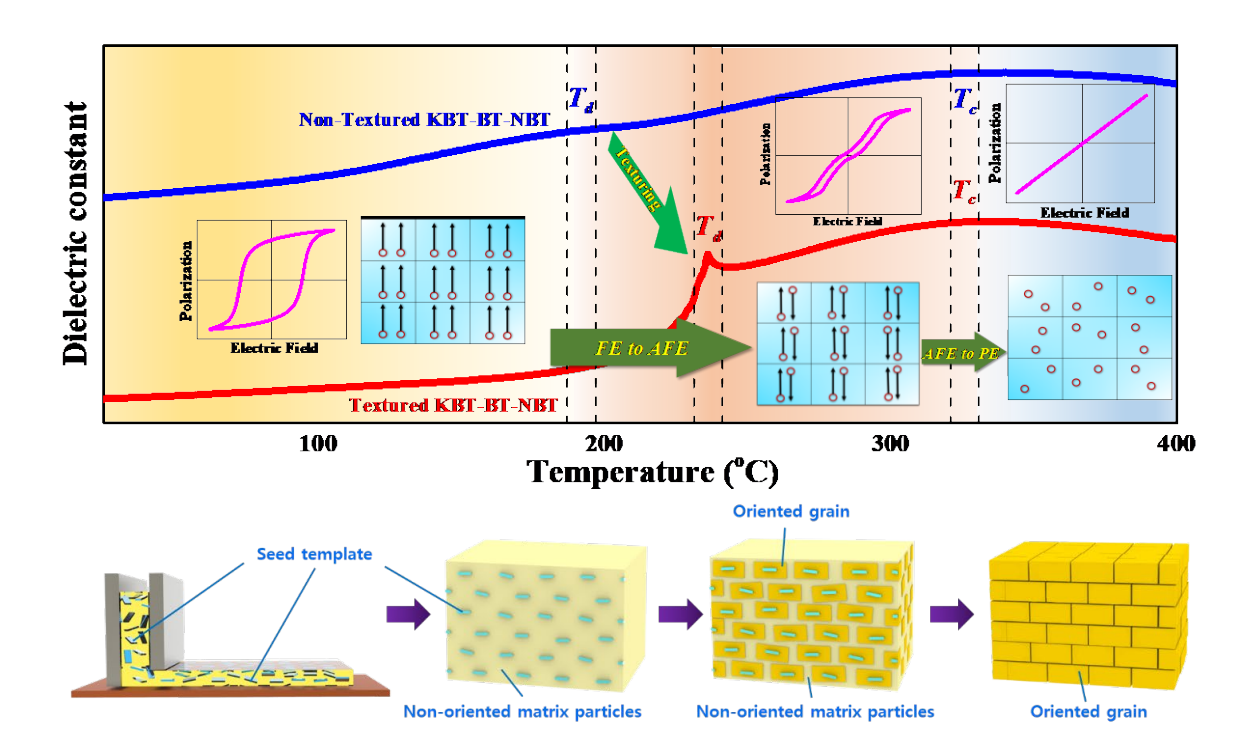


Fig. 1. (a) Schematic illustration of the texture-driven sharp ferroelectric to antiferroelectric phase transition in the KBT-BT-NBT ceramic, which results in a giant pyroelectric coefficient near the transition temperature regime. (b) Schematics of the synthesis mechanism of the [001]_{pc}-oriented KBT-BT-NBT ceramic. BaTiO₃ (BT) single crystal platelets synthesised by the topochemical microcrystal conversion method were used as seed templates in the ferroelectric ceramic matrix. The texturing process involves sequential steps, viz., tape casting to align the seeds, lamination of tapes, binder burnout at 400 °C, and sintering at 1150 °C for 50 h to induce the epitaxial grain growth.

2. Materials and method

2.1 Specimen design

The random and textured KBT-BT-NBT (0.2(2/3K_{0.5}Bi_{0.5}TiO₃–1/3BaTiO₃)-0.8Na_{0.5}Bi_{0.5}TiO₃) tetragonal-phase lead-free FE ceramics were synthesised by the conventional solid-state route and TGG method, respectively (**Fig. 1b**). BaTiO₃ (BT) single crystal platelets synthesised by a topochemical microcrystal conversion method [30,31] were employed as seed templates in the ceramic matrix slurry, followed by tape casting with a doctor blade to align the distribution of seeds. After the binder burnout process (400 °C for 4 h), the green body was heated at 1150 °C for 50 h to induce grain texturing. The details of the synthesis process are provided elsewhere [32].

2.2 Experimental methods

The morphology of the samples was analysed using a LEO Zeiss 1550 (Zeiss, Munich, Germany) scanning electron microscope. To investigate the degree of orientation, electron backscatter diffraction (EBSD) orientation mapping was performed on the textured and random KBT-BT-NBT ceramics using an EBSD detector (Nord-Lys-NANO, Oxford instrument). The X-ray diffraction patterns of the ceramics were recorded at RT using a PANalytical X'pert PRO X-ray diffractometer with monochromatic Cu $K\alpha$ radiation (λ = 1.5406 Å). The FE domain patterns of the ceramics were analysed by piezoresponse force microscopy (PFM) on a commercial atomic force microscope (AFM; NX-10, Park Systems). The PFM was performed with Pt/Cr conductive coated tips (Multi75E-G, BudgetsSensors) and a lock-in amplifier (SR830, Stanford Research Systems) by applying a voltage of 4 V_{ac} at 17 kHz to the AFM tip. For electrical measurements, Ag electrodes were applied on the flat surfaces of rectangular specimens. The Polarization vs.

electric field (*P–E*) loop measurement was performed using a FE evaluation system (TF2000, aixACCT) at different temperatures between 25 and 240 °C. The ceramic samples were poled at 5 kV/mm at room temperature for 10 min. The temperature-dependent dielectric properties of the poled samples were evaluated using an impedance analyser (E4990A, Keysight Technology) coupled with a test furnace in the temperature range of 20 to 400 °C. The pyroelectric response was measured over the temperature range of 25–250 °C at a constant heating rate of 1 °C/min. For this, a Keithley electrometer (6517B) was coupled with a high-temperature test oven (PolyK Tech., PA, USA) and interfaced via the LabView software.

3. Results and discussion

3.1 Crystallographic and morphological analysis

The crystallographic phase and the degree of texturing of the [001]-textured KBT-BT-NBT ceramic were evaluated using the XRD patterns collected at RT (**Fig. 2a**). The XRD pattern of the textured ceramic shows strong $\{200\}_{pc}$ Bragg reflections ((200) and (002) peaks), confirming a predominant tetragonal phase with polarization vector parallel to the [001] direction. The decreased intensity of the $(110)_{pc}$ peak and the increased intensities of the $(001)_{pc}$ and $(002)_{pc}$ peaks clearly indicate a high degree of texturing along the [001] direction [27]. The texturing degree of the ceramic was determined from the XRD pattern obtained in the range of $2\theta = 20^{\circ}$ to 60° by employing Equation 2 (the Lotgering method [33]). The Lotgering factor (*LF*) is expressed as,

$$LF_{00l} = \frac{P - P_0}{1 - P_0} where, P = \frac{\sum I(00l)}{\sum I(hkl)}, P_0 = \frac{\sum I_0(00l)}{\sum I_0(hkl)}.$$
 (2)

Here, I and I_0 are the intensities of the XRD peaks of the textured and non-textured ceramics, respectively. The LF of the textured KBT-BT-NBT ceramic was calculated to be 93 % using Equation 2. The surface morphology of the ceramics was analysed by SEM (**Fig. 2b and c**). It is clear that the non-textured ceramic has an average grain size of <1 μ m. Meanwhile, the textured ceramic sample has a larger grain size of ~10–15 μ m. In the TGG process, the grain growth rate of the matrix depends on the difference in the size of the template seed crystals and matrix grain size. Larger template seed crystals are energetically more stable than smaller matrix grains. This leads to diffusion and then the dissolution of smaller grains at the surface of the seed crystals, resulting in a continuous growth to large grains oriented along the crystallographic direction of the seed surface.

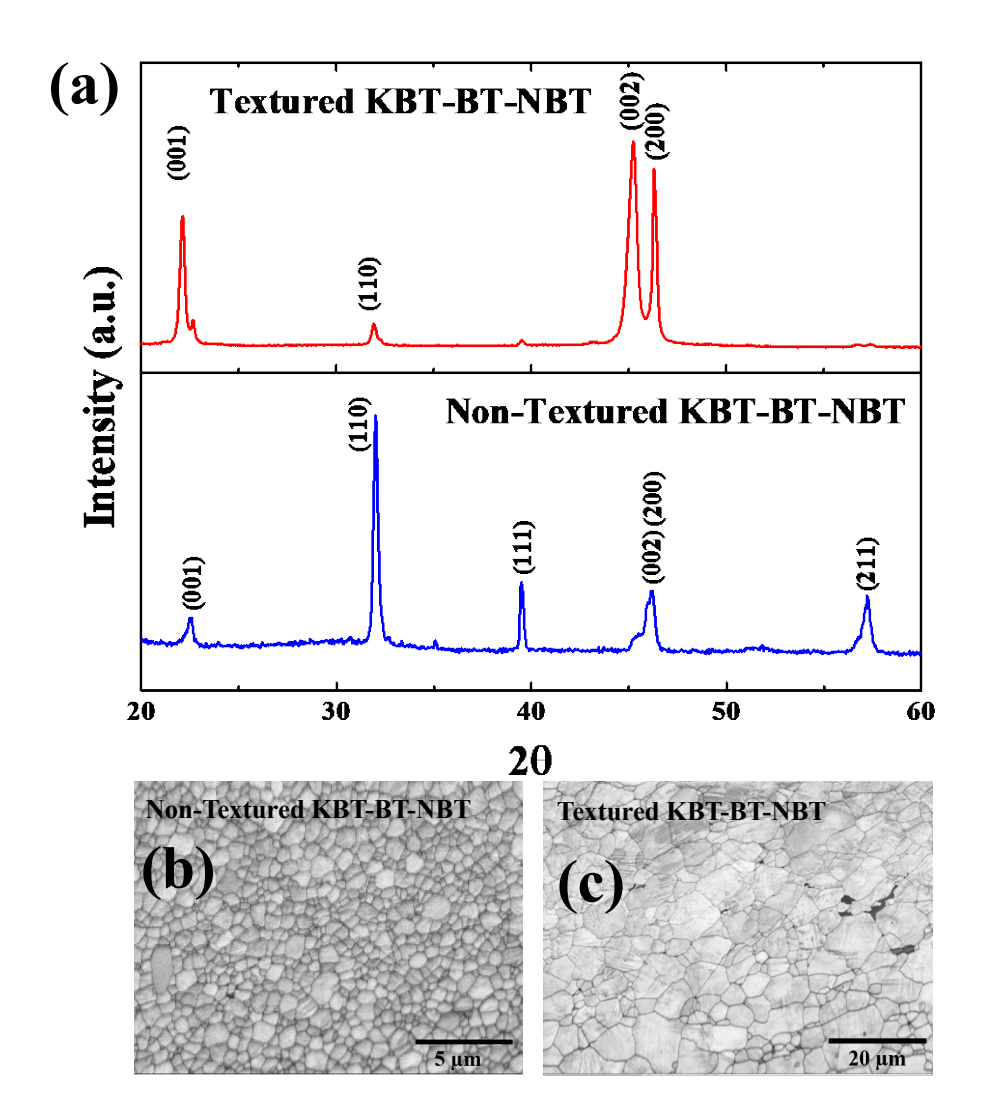


Fig. 2. (a) Comparison of the XRD patterns of non-textured (or random) and textured KBT-BT-NBT ceramics. The spilt in peaks of the {200}_c Braggs reflection clearly demonstrates the presence of tetragonal symmetry. SEM micrographs of the (b) non-textured and (c) textured KBT-BT-NBT ceramics show the comparatively larger grain size of the textured ceramic.

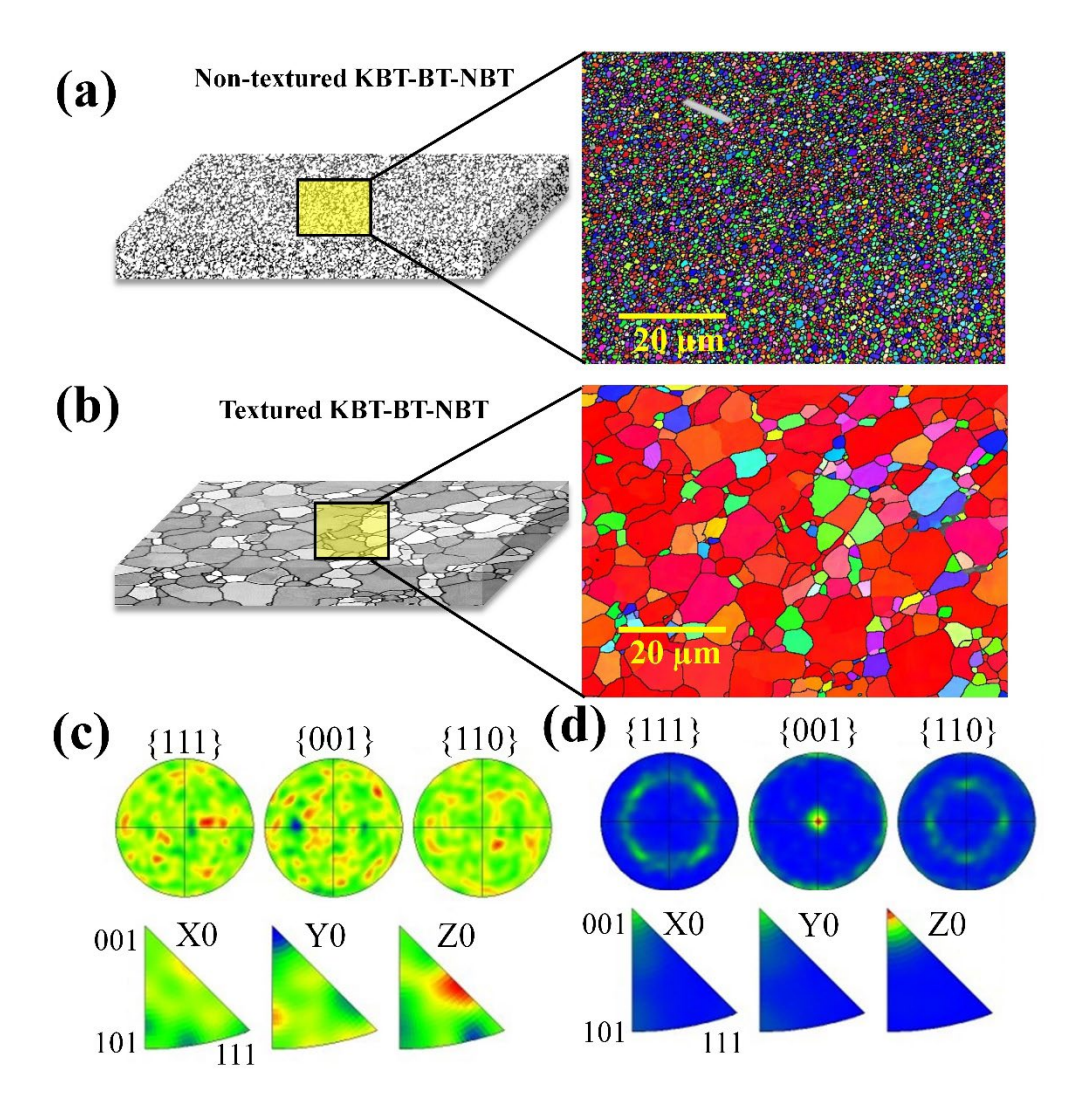


Fig. 3. Schematic representation of (a) non-textured and (b) [001]_{pc}-textured KBT-BT-NBT ceramics with the highlighted area of investigation and the respective EBSD orientation maps. The larger grains of size 10–15 μm aligned in the [001] direction clearly suggest a high degree of texturing (LF of 93 %) in the textured sample. The pole figures and inverse pole figures of the [111], [001], and [110] orientations for the (c) non-textured and (d) textured ceramics.

To further investigate the morphology and spread of oriented grains in the textured KBT-BT-NBT ceramic, EBSD images and pole figures were obtained (**Fig. 3**). The EBSD images clearly show that the grains are oriented along the [001] direction in the textured ceramic in

contrast with those in the randomly oriented grains in the non-textured sample (colour maps become uniform). Fig. 3c and d show the colour representation of the crystallographic planes of the non-textured and textured KBT-BT-NBT ceramics, respectively. The pole figures of the textured ceramic clearly show the [001] axis parallel to the perpendicular direction of the plane, which is also supported by the XRD patterns.

3.2 Dielectric analysis

Although the depolarization temperature (T_d) is an important parameter and plays a crucial role in the pyroelectric response of FE materials, its origin is still not well understood for NBT-BT-based ceramics. T_d is generally defined as the temperature at which a steep decrement in the remanent polarization occurs. Zhang et al. termed it as the temperature corresponding to the FE to relaxor phase transition; this subject, however, continues to be debated in the research community [34]. In this study, T_d was determined by two methods, viz., analyses of the temperature-dependent dielectric response and P-E hysteresis. The temperature-dependent dielectric constant (ε_r) and loss tangent $(tan\delta)$ of the non-textured and textured ceramics are shown in Fig. 4a and 4b, respectively. The textured KBT-BT-NBT ceramic sample shows a sharp transition peak at 235 °C in both the dielectric constant and loss tangent curves, whereas in the case of the non-textured ceramic, a diffused transition with a broad shoulder is observed between 100 and 200 °C without a clearly identifiable transition temperature. It can also be noted here that the ε_r and $tan\delta$ values decrease after the texturing of the ceramic. The decrement in ε_r and $tan\delta$ significantly improves the FoM values of the ceramic. To analyse the phase transition behaviours in detail, we obtained temperature-dependent P-E hysteresis loops at 1 Hz over a wide temperature range (25 to 250 °C), which are shown in **Fig. 4c.d**.

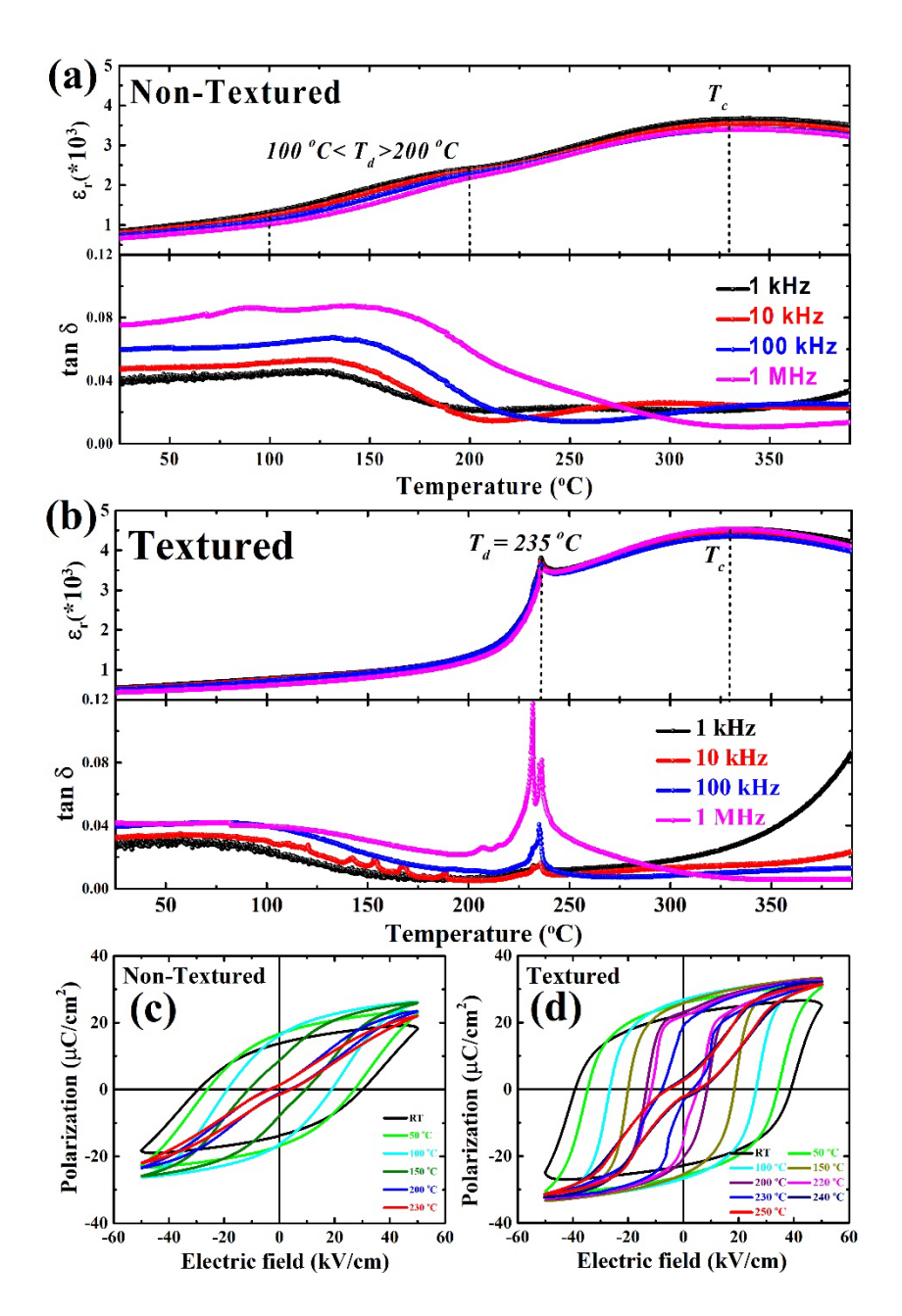


Fig. 4. Relative permittivity (ε_r) and loss tangent ($tan\delta$) vs. temperature over a wide frequency range (1 kHz to 10 MHz) for (a) non-textured and (b) textured KBT-BT-NBT ceramics. The depolarization temperature (T_d) is observed at 235 °C for textured ceramic. P-E hysteresis loops of the (c) non-textured and (d) textured ceramics over a wide temperature range (25 to 250 °C). The textured ceramic exhibits abrupt and strong FE to AFE phase transition between 230 and 240 °C, which results in a giant pyroelectric coefficient due to high dP_r/dT .

3.3 Analysis of the FE behaviour

At RT, the P-E loops of both types of ceramics show a high coercive field and typical square shape observed for FE materials. The remanent polarization (P_r) of the textured sample is comparatively higher than that of the non-textured sample owing to the high degree of texturing. The non-textured ceramic shows a nearly linear decrease in the P_r and coercive field (E_c) with respect to the temperature up to 100 °C and exhibits a pinched slim hysteresis loop at a high temperature of 200 °C. This indicates a gradual FE-AFE phase transition over a wide temperature range (100 to 200 °C), where FE and AFE phases coexist. Similar behaviours were reported by Zhang et al. and Guo et al. [35,36]. For textured ceramic specimens, a typical FE hysteresis loop with high P_r values was observed up to 220 °C. However, the P_r value decreased abruptly as the temperature exceeded ~230 °C, whereas the maximum polarization (P_{max}) remained nearly unchanged, resulting in a pinched *P–E* hysteresis loop at 240 °C. This confirms the rapid and sharp FE-AFE phase transition of the textured specimen at 235 °C. Additionally, because the textured ceramic possesses larger and ordered domains compared to the smaller and random distribution of the domains of the non-textured ceramic, it shows larger spontaneous polarization than that of the non-textured ceramic. In addition, owing to the presence of high quantities of larger FE domains and the corresponding 180° domain switching, a higher temperature is required to completely depolarize the ceramic, leading to a higher T_d .

3.4 Ferroelectric domain structure analysis

To understand the microscopic origin of the difference between the FE-AFE transition behaviours of the non-textured and textured samples, the FE domain analysis was conducted by PFM (Fig. 5) [37]. It can be clearly observed in Fig. 5 that the non-textured ceramic shows a

random distribution of small domains with a small portion of the out-of-plane component. In contrast, the domain morphology of the textured KBT-BT-NBT ceramic exhibits clear stripe-shaped patterns at the micrometer scale with a relatively large portion of the out-of-plane component, which can be also found in Fig. 5e,f. Furthermore, the line profiles of the PFM piezoresponse (Fig. 5e,f) indicate that the size distribution of the domains is much more uniform in the textured sample than in the non-textured sample. The texturing of the KBT-BT-NBT ceramic greatly enhances the size of grains (10–15 μm) that are aligned along the [001] direction. The enhanced domain size under texture engineering as compared with that of the non-textured counterpart can be attributed to the larger grain size [38,39].

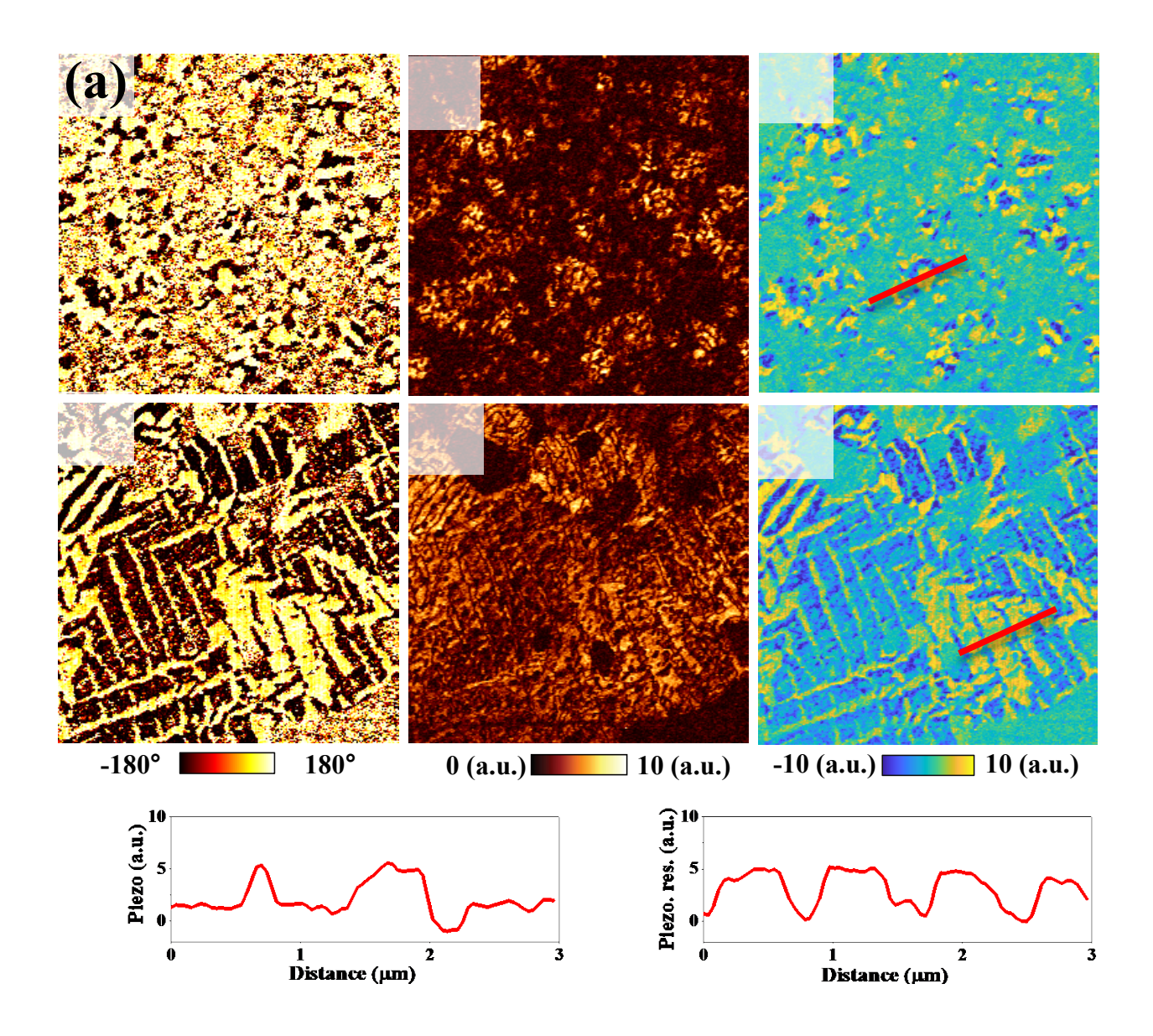


Fig. 5. (a, b) PFM phase, (c, d) PFM amplitude, (e, f) PFM piezoresponse [amplitude * $\cos(\text{phase})$], and (g, h) the corresponding piezoresponse line profiles of the 10 μ m \times 10 μ m area of the non-textured and textured KBT-BT-NBT ceramics, respectively. The PFM phase image of the non-textured ceramic clearly shows random domains, whereas the textured ceramics shows much larger stripe-patterned domains. The tetragonal crystallographic phase provides an excellent path for easier 180° domain switching, which results in giant pyroelectricity.

The uniform distribution of large FE domains contributes to enhanced net polarization. [40]. Li et al. reported that the tetragonal crystallographic symmetry of FE polycrystalline ceramics allows the easier switching of the 180° domains [41]. As the 180° polarization switching is a prime parameter in the FE-AFE phase transition, the phase transition behaviour of the textured and nontextured samples is considered to be closely related to their 180° domain switching characteristics. Because the electrode is formed parallel to the (001) plane in the textured sample, the polarization change due to the 180° domain can be measured as fully contributing. The abrupt and strong phase transition of the textured sample indicates a coherent switching of 180° domains with a tetragonal symmetry. On the other hand, the broad and diffused phase transition of the non-textured sample suggests that the 180° domain switching rate is locally different, that is, the deviation in the energy required for the dipole switching is relatively large throughout the sample. These different switching behaviours of the textured and non-textured samples directly affect their FE-AFE phase equilibrium temperature (T_d) . For the textured sample, owing to the [001]-oriented large tetragonal grains with uniformly distributed large domains, the 180° polarization switching can take place coherently throughout the sample in the narrow FE-AFE phase equilibrium temperature range, resulting in a sharp T_d peak in Fig. 4b. However, the non-textured ceramic possesses nondistinct and randomly distributed small domains with randomly oriented small grains; therefore, the geometrical restrictions and internal stresses affecting the ionic displacement are inevitably larger than in the case of textured ceramic. Furthermore, the switching and movement of the FE domain walls are limited by the smaller grain size due to the dominant pinning centres. This might cause a local difference in the resultant rate of 180° polarization switching, thereby causing an expansion of the FE-AFE phase equilibrium temperature range, and leading to a broad T_d shoulder in Fig. 4a.

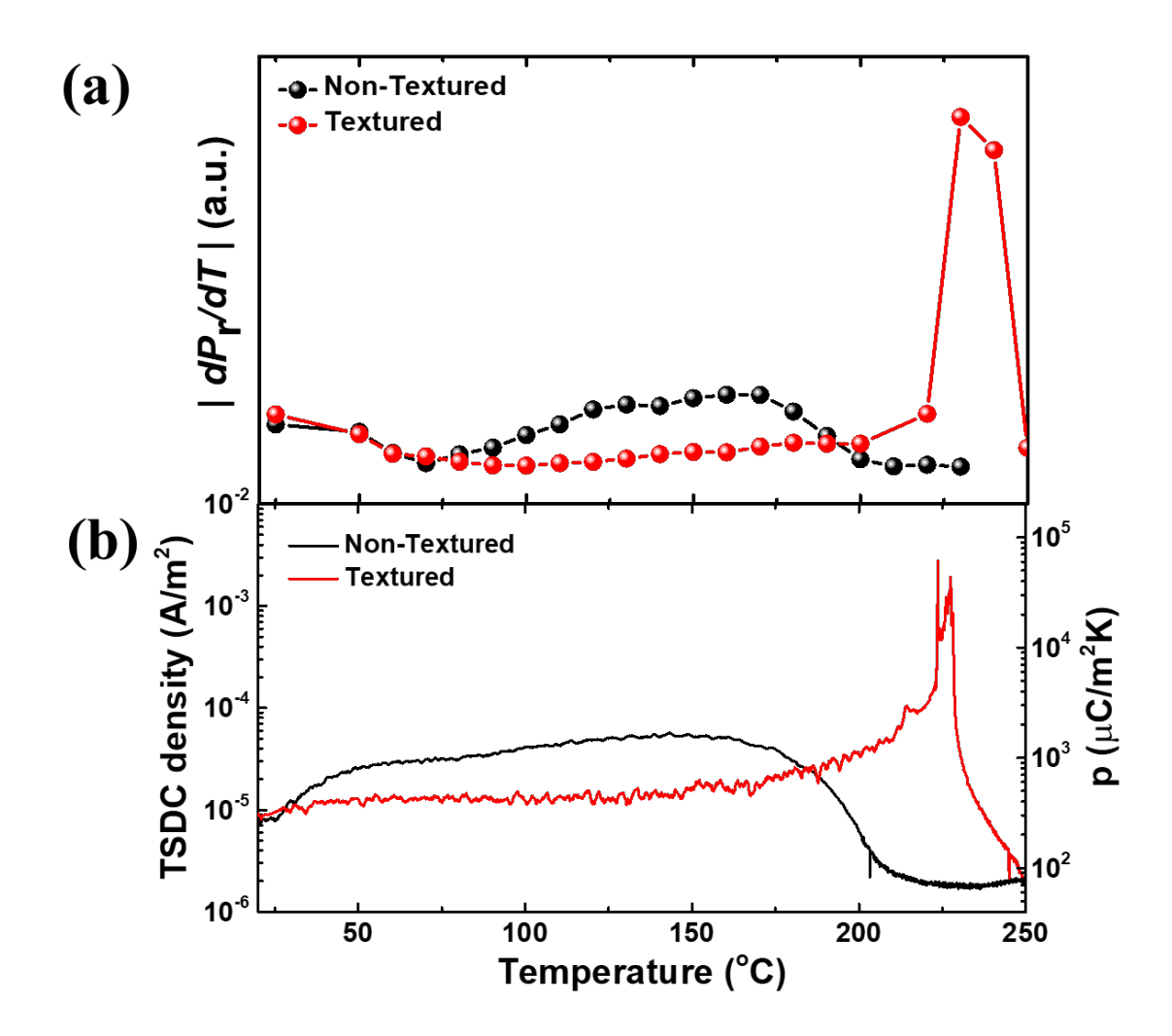


Fig. 6. (a) Slope of the remanent polarization with temperature plot ($|dP_r/dT|$) for textured and non-textured ceramics over a wide temperature range (25–250 °C), which clearly demonstrates a high slope at 235 °C for textured ceramic, corresponding to the giant pyroelectric coefficient. (b) Temperature-dependent pyroelectric TSDC density semilogarithmic plots in the range of 25 to 250 °C for the KBT-BT-NBT ceramics, which clearly demonstrate the impact of texturing on the large enhancement in the pyroelectric response. The right-side y-axis of the plot shows the corresponding calculated pyroelectric coefficients from TSDC density for both ceramics.

3.5 Analysis of the pyroelectric response

The narrow FE-AFE phase equilibrium temperature range (or sharp FE-AFE phase transition peak) was found to be critical for maximising the rate of change in P_r with respect to the temperature $(dP_r/dT, directly reflecting the pyroelectric performance given by Equation 1). As$ shown in Fig. 6a, the textured sample exhibited a sharp peak at 235 °C (T_d), whereas the nontextured ceramic shows a broad peak near the 100 to 200 °C temperature range. This broad temperature range corresponds to the broad FE-AFE phase equilibrium temperature range of the non-textured sample, over which the fraction of the FE phase gradually decreases as the temperature increases; consequently, the P_r value also decreases gradually (Fig. 4c). The pyroelectric response shown in Fig. 6b was obtained using the TSDC measurement system, which is a direct method for evaluating the pyroelectric characteristics; in this system, the heating rate was kept constant at 1 °C/min. In view of this, for the FoM calculations, we considered the pyroelectric coefficient values calculated from the TSDC measurement system. Further, it should be noted that there is a difference between the pyroelectric response patterns in Fig. 6a and b, which can be attributed to the heating rate difference in the temperature-dependent P-E measurement. Fig. 6b shows the pyroelectric response of both samples evaluated by measuring the TSDC density (J_{TSDC}) in the temperature range of 25 to 250 °C with a uniform heating rate of 1 °C/min. As expected, the trend of the measured J_{TSDC} was similar to that of dP_r/dT . The KBT-BT-NBT textured ceramic exhibited a significant enhancement over the non-textured ceramic in the pyroelectric coefficient, p, from 258 to 326 μ C m⁻² K⁻¹ at RT. Meanwhile, at the T_d (235 °C), the corresponding coefficient, that is, the p_{TSDC} (coefficient calculated from J_{TSDC}) value increases from 57 to 90900 μ Cm⁻²K⁻¹. Also, the non-textured ceramic exhibited it's maximum p_{TSDC} of 1750 $\mu \text{Cm}^{-2} \text{K}^{-1}$ at 150 °C (i.e. T_d for non-textured ceramic). It is interesting to note that the RT

pyroelectric coefficient (326 μ Cm⁻²K⁻¹) is comparable to that of the doped lead-containing pyroelectric ceramics. It should be emphasized that these pyroelectric coefficients were calculated from the TSDC measurement performed on heating only. Such TSDC values may also have contributions from the release of trapped charges and non-reversible effects due to domain wall motions. The latter effects are likely to occur near T_d and generally account for the very large coefficients in this region. Thus, the RT pyroelectric coefficients used for the calculations of the *FoM* values were not demonstrated experimentally to be truly reversible values, which would also need measurements on cooling to verify them and should only be taken as indicative values at this stage.

The above discussions clearly demonstrate that the domain engineering of KBT-BT-NBT ceramics using the TGG method is a powerful way to enhance the pyroelectric effect by controlling the FE–AFE phase transition behaviours. To evaluate the pyroelectric materials for specific applications, their FOM parameters such as the current responsivity, F_i ; voltage responsivity, F_v ; and detectivity, F_D , are important [29]. The FoM values are estimated based on the obtained values of p_{TSDC} , dielectric permittivity, loss tangent obtained at 100 Hz, and volume-specific heat. Depending on the specific pyroelectric application, the corresponding FoM is considered. For example, for infra-red applications such as IR sensing, current responsivity (F_i) and detectivity (F_D) are important. Likewise, to evaluate the material at a large pyroelectric voltage, the voltage responsivity (F_v) is considered. In this study, F_i , F_v , and F_D were calculated for the synthesised ceramics, and they are listed in Table 1. The FoM values were calculated based on Equations (3) to (5).

$$F_i = \frac{p}{C_v} \tag{3}$$

$$F_{v} = \frac{p}{C_{v} \varepsilon_{0} \varepsilon_{r}} \tag{4}$$

$$F_D = \frac{p}{[C_v](\varepsilon_r \varepsilon_0 \tan \delta)^{1/2}]}$$
 (5)

here, C_v is the volume-specific heat (2.8 J K⁻¹ cm⁻³ for NBT-BT ceramics [42]), and ε_o , ε_r , and $tan\delta$ are the absolute permittivity of vacuum, relative permittivity, and dielectric loss, respectively. As shown in Table 1, the p_{TSDC} and FoM values (F_i , F_v , and F_D) at RT for the textured KBT-BT-NBT ceramic are comparable with the values reported previously for different ceramics [8,22,41-44]. The F_i value increased significantly (by nearly 2 times at RT) for the textured ceramic as compared to that of the non-textured ceramic.

Table 1. Comparison of the calculated coefficient (p_{TSDC}) at RT and the corresponding FoM values (F_i , F_v and F_D) of the non-textured and textured (1–x)KBT-BT-xNBT ceramics with the values reported for other ceramics.

S.N.	Ceramic		ε _r (100 Hz)	tanδ	<i>p_{TSDC}</i> (μCm K)	F_{i} (10 mV)	F _v (m C)	F_D (10-5Pa-1/2)	Ref.
1.	0.2KBT -BT-	Non-Textured	660	0.23	258	0.92	0.015	0.53	This work
	0.8NBT	Textured	566	0.01	326	2.06	0.035	1.64	WOIK
2.	Ba _{0.85} Sr _{0.15} Ti _{0.9} Zr _{0.1} O ₃		4691	0.041	1400	0.6	0.015	1.45	[43]
3.	0.94(Bi _{0.5} Na _{0.5})TiO ₃ - 0.06Ba(Ti _{0.75} Zr _{0.25})O ₃		1462 (1 kHz)	0.046	2720	9.71	0.075	3.98	[44]
4.	PZT		1990	0.014	414	1.42	0.008	0.9	[45]
5.	NBT-0.06BT		396 (1 kHz)	0.04	315	1.12	0.021	9.08	[23]
6.	0.005La-NBT-0.06BT- 0.002Ta		671 (1 kHz)	0.047	1292	4.61	0.078	2.76	[23]
7.	LaTiO ₃		47	0.005	230	0.71	0.17	4.9	[8]

8.	PZFNTU	290	0.003	380	1.52	0.06	5.8	[46]

4. Conclusions

The enhancement of the pyroelectric response of the grain-oriented lead-free KBT-BT-NBT ceramic synthesised by the TGG process was demonstrated. The coefficients estimated from the pyroelectric response measured (J_{TSDC}) at depolarization temperature (235 °C) are 57 and 90900 μ Cm⁻²K⁻¹ for non-textured and textured ceramics, respectively. The large pyroelectric response is attributed to the sharp FE to AFE phase transition driven by the crystallographic texture at T_d , which is influenced by the increased size and uniform distribution of the FE domains. Additionally, the pyroelectric FoM values such as the current responsivity (F_t), voltage responsivity (F_v), and detectivity (F_D), were also significantly enhanced at RT, only by the texturing of the ceramic. The pyroelectric response and FoM values, at T_d and RT, of the textured sample were found to be higher than those of some other reported lead-based FEs, such as PZT and other derivatives; these features make it a possible choice for pyroelectric sensors and thermal energy harvesting applications. Thus, this study clearly demonstrates the impact of texturing on the pyroelectricity and opens a new pathway for exploiting the FE phase transition (FE to AFE) to achieve an enhanced pyroelectric response in polycrystalline ceramics.

ACKNOWLEDGMENTS

This study was supported by the National Research Council of Science & Technology (NST) grant by the Korean government (MSIP) (No. CAP-17-04-KRISS), the National Research Foundation of Korea (NRF-2019R1A2B5B01070100) and "Human Resources Program in Energy Technology" of the Korea Institute of Energy Technology Evaluation and Planning (KETEP), and granted financial resource from the Ministry of Trade, Industry & Energy, Republic of Korea (No.

20174030201800). H.-C. Song acknowledges the support from the Energy Technology Development Project (KETEP) grant funded by the Ministry of Trade, Industry and Energy, Republic of Korea (2018201010636A) and the Korea Institute of Science and Technology (2E30410). K.-H. Cho acknowledges the support from the National Research Foundation (NRF) of Korea funded by the Ministry of Education (NRF-2018R1A6A1A03025761 and NRF-2019R1I1A3A01058105). S.P. acknowledges the financial support from the National Science Foundation through award number 1936432.

CONFLICT OF INTEREST

The authors declare no conflicts of interest.

REFERENCES

- [1] R. Levin, M.J. Brown, M.E. Kashtock, D.E. Jacobs, E.A. Whelan, J. Rodman, M.R. Schock, A. Padilla, T. Sinks, Lead exposures in U.S. children, 2008: Implications for prevention, Environ. Health Perspect. 116 (2008) 1285–1293.
- [2] I.W. Donald, Waste Immobilization in Glass and Ceramic Based Hosts: Radioactive,Toxic and Hazardous Wastes, 2010.
- [3] A. Kumar, J.Y. Yoon, A. Thakre, M. Peddigari, D.Y. Jeong, Y.M. Kong, J. Ryu, Dielectric, ferroelectric, energy storage, and pyroelectric properties of Mn-doped (Pb_{0.93}La_{0.07})(Zr_{0.82}Ti_{0.18})O₃ anti-ferroelectric ceramics, J. Korean Ceram. Soc. 56 (2019) 412–420.
- [4] H. He, X. Lu, E. Hanc, C. Chen, H. Zhang, L. Lu, Advances in lead-free pyroelectric materials: a comprehensive review, J. Mater. Chem. C. 8 (2020) 1494-1516.

- [5] M. Shen, Y. Qin, Y. Zhang, M.A. Marwat, C. Zhang, W. Wang, M. Li, H. Zhang, G. Zhang, S. Jiang, Enhanced pyroelectric properties of lead-free BNT-BA-KNN ceramics for thermal energy harvesting, J. Am. Ceram. Soc. 102 (2019) 3990–3999.
- [6] A. Thakre, A. Kumar, D.-Y. Jeong, G.-T. Hwang, W.-H. Yoon, H.-Y. Lee, J. Ryu, Enhanced Mechanical Quality Factor of 32 Mode Mn Doped 71Pb(Mg_{1/3}Nb_{2/3})O₃–29PbZrTiO₃ Piezoelectric Single Crystals, Electron. Mater. Lett. 16 (2020) 156–163.
- [7] Q. Xu, X. Zhao, X. Li, L. Li, L. Yang, W. Di, J. Jiao, H. Luo, Novel electrode layout for relaxor single crystal pyroelectric detectors with enhanced responsivity and specific detectivity, Sensors Actuators A Phys. 234 (2015) 82–86.
- [8] R.W. Whatmore, Pyroelectric devices and materials, Reports Prog. Phys. 49 (1986) 1335–1386.
- [9] J. Gao, X. Hu, L. Zhang, F. Li, L. Zhang, Y. Wang, Y. Hao, L. Zhong, X. Ren, Major contributor to the large piezoelectric response in (1–x)Ba(Zr_{0.2}Ti_{0.8})O₃–x(Ba_{0.7}Ca_{0.3})TiO₃ ceramics: Domain wall motion, Appl. Phys. Lett. 104 (2014) 252909.
- [10] B. Jimenez, C. Alemany, J. Mendiola, E. Maurer, Phase transitions in ferroelectric ceramics of the type Sr_{0.5}Ba_{0.5}Nb₂O₆, J. Phys. Chem. Solids. 46 (1985) 1383–1386.
- [11] C. Zhou, Q. Li, J. Xu, L. Yang, W. Zeng, C. Yuan, G. Chen, Ferroelectric-quasiferroelectric-ergodic relaxor transition and multifunctional electrical properties in Bi_{0.5}Na_{0.5}TiO₃-based ceramics, J. Am. Ceram. Soc. 101 (2018) 1554–1565.
- [12] G. Han, C.W. Ahn, J. Ryu, W.H. Yoon, J.J. Choi, B.D. Hahn, J.W. Kim, J.H. Choi, D.S.

- Park, Effect of tetragonal perovskite phase addition on the electrical properties of KNN thick films fabricated by aerosol deposition, Mater. Lett. 65 (2011) 2762–2764.
- [13] J. Ryu, J.J. Choi, B.D. Hahn, D.S. Park, W.H. Yoon, K.Y. Kim, Sintering and piezoelectric properties of KNN ceramics doped with KZT, in: IEEE Trans. Ultrason. Ferroelectr. Freq. Control. 54 (2007) 2510–2515.
- [14] J. Rödel, W. Jo, K.T.P. Seifert, E.-M. Anton, T. Granzow, D. Damjanovic, Perspective on the Development of Lead-free Piezoceramics, J. Am. Ceram. Soc. 92 (2009) 1153–1177.
- [15] W. Liu, X. Ren, Large Piezoelectric Effect in Pb-Free Ceramics, Phys. Rev. Lett. 103 (2009) 257602.
- [16] H.P. Kim, C.W. Ahn, Y. Hwang, H.Y. Lee, W. Jo, Strategies of a potential importance, making lead-free piezoceramics truly alternative to PZTs, J. Korean Ceram. Soc. 54 (2017) 86–95.
- [17] F. Cordero, F. Craciun, F. Trequattrini, E. Mercadelli, C. Galassi, Phase transitions and phase diagram of the ferroelectric perovskite (Na_{0.5}Bi_{0.5})1–xBaxTiO₃ by anelastic and dielectric measurements, Phys. Rev. B. 81 (2010) 144124.
- [18] W.H. Chan, Z. Xu, J. Zhai, H. Chen, Uncooled tunable pyroelectric response of antiferroelectric Pb_{0.97}La_{0.02}(Zr_{0.65}Sn_{0.22}Ti_{0.13})O₃ perovskite, Appl. Phys. Lett. 87 (2005) 1–3.
- [19] N.M. Shtykov, J.K. Vij, V.P. Panov, R.A. Lewis, M. Hird, J.W. Goodby, Observation of an SmC(α) phase in an antiferroelectric liquid crystal using pyroelectrics and dielectrics, J.

- Mater. Chem. 9 (1999) 1383-1385.
- [20] L. Li, R.X. Wang, M. Shen, H. Zhang, Z. Bin Gu, S.T. Zhang, D. Wu, Phase/domain structure and enhanced thermal stable ferro-/pyroelectric properties of (1-x)0.94Na_{0.48}Bi_{0.44}TiO₃-0.06BaTiO₃:xZnO ceramics, J. Eur. Ceram. Soc. 40 (2020) 699–705.
- [21] H. Luo, H. Ke, H. Zhang, L. Zhang, F. Li, L. Cao, D. Jia, Y. Zhou, Enhanced ferroelectric and energy-storage properties of Nb-doped 0.94Na_{0.5}Bi_{0.5}TiO₃-0.06BaTiO₃ ceramics prepared by a multi-ionic sol-gel method, Phys. B Condens. Matter. 567 (2019) 17–24.
- [22] A.M. Balakt, C.P. Shaw, Q. Zhang, Enhancement of pyroelectric properties of lead-free 0.94Na_{0.5}Bi_{0.5}TiO₃-0.06BaTiO₃ ceramics by La doping, J. Eur. Ceram. Soc. 37 (2017) 1459–1466.
- [23] A.M. Balakt, C.P. Shaw, Q. Zhang, Giant pyroelectric properties in La and Ta co-doped lead-free 0.94Na_{0.5}Bi_{0.5}TiO₃ 0.06BaTiO₃ ceramics, J. Alloys Compd. 709 (2017) 82–91.
- [24] R. Sun, J. Wang, F. Wang, T. Feng, Y. Li, Z. Chi, X. Zhao, H. Luo, Pyroelectric properties of Mn-doped 94.6Na_{0.5}Bi_{0.5}TiO₃-5.4BaTiO₃ lead-free single crystals, J. Appl. Phys. 115 (2014) 074101.
- [25] H. Cao, B. Fang, H. Xu, H. Luo, Crystal orientation dependence of dielectric and piezoelectric properties of tetragonal Pb(Mg_{1/3}Nb_{2/3})O₃-38%PbTiO₃ single crystal, Mater. Res. Bull. 37 (2002) 2135–2143.
- [26] S. Zhukov, Y.A. Genenko, J. Koruza, J. Schultheiß, H. von Seggern, W. Sakamoto, H.

- Ichikawa, T. Murata, K. Hayashi, T. Yogo, Effect of texturing on polarization switching dynamics in ferroelectric ceramics, Appl. Phys. Lett. 108 (2016) 012907.
- [27] D. Maurya, Y. Zhou, Y. Wang, Y. Yan, J. Li, D. Viehland, S. Priya, Giant strain with ultra-low hysteresis and high temperature stability in grain oriented lead-free K_{0.5}Bi_{0.5}TiO₃-BaTiO₃-Na_{0.5}Bi_{0.5}TiO₃ piezoelectric materials, Sci. Rep. 5 (2015) 8595.
- [28] F. Guo, B. Yang, S. Zhang, F. Wu, D. Liu, P. Hu, Y. Sun, D. Wang, W. Cao, Enhanced pyroelectric property in (1–x)(Bi_{0.5}Na_{0.5})TiO₃-xBa(Zr_{0.055}Ti_{0.945})O₃: Role of morphotropic phase boundary and ferroelectric-antiferroelectric phase transition, Appl. Phys. Lett. 103 (2013) 182906.
- [29] A. Thakre, A. Kumar, H.C. Song, D.Y. Jeong, J. Ryu, Pyroelectric energy conversion and its applications—flexible energy harvesters and sensors, Sensors (Switzerland). 19 (2019) 19092170.
- [30] Y. Saito, H. Takao, K. Wada, Synthesis of platelike CaTiO₃ particles by a topochemical microcrystal conversion method and fabrication of textured microwave dielectric ceramics, Ceram. Int. 34 (2008) 745–751.
- [31] L. Liu, R. Lv, Z. Guo, Y. Wang, Fabrication of Columnar NaNbO₃-Based Particles

 Through Topochemical Microcrystal Conversion, Electron. Mater. Lett. 16 (2020) 55–60.
- [32] D. Maurya, Y. Zhou, Y. Yan, S. Priya, Synthesis mechanism of grain-oriented lead-free piezoelectric Na_{0.5}Bi_{0.5}TiO₃–BaTiO₃ ceramics with giant piezoelectric response, J. Mater. Chem. C. 1 (2013) 2102.

- [33] R. Furushima, S. Tanaka, Z. Kato, K. Uematsu, Orientation distribution-Lotgering factor relationship in a polycrystalline material-as an example of bismuth titanate prepared by a magnetic field, J. Ceram. Soc. Japan. 118 (2010) 921–926.
- [34] S.-T. Zhang, A.B. Kounga, E. Aulbach, W. Jo, T. Granzow, H. Ehrenberg, J. Rödel, Lead-free piezoceramics with giant strain in the system Bi_{0.5}Na_{0.5}TiO₃–BaTiO₃–K_{0.5}Na_{0.5}NbO₃.

 II. Temperature dependent properties, J. Appl. Phys. 103 (2008) 034108.
- [35] S.T. Zhang, A.B. Kounga, E. Aulbach, H. Ehrenberg, J. Rödel, Giant strain in lead-free piezoceramics Bi_{0.5}Na_{0.5}TiO₃-BaTiO₃-K_{0.5}Na_{0.5}NbO₃ system, Appl. Phys. Lett. 91 (2007) 112906.
- [36] S.T. Zhang, A.B. Kounga, E. Aulbach, T. Granzow, W. Jo, H.J. Kleebe, J. Rödel, Lead-free piezoceramics with giant strain in the system Bi_{0.5}Na_{0.5}TiO₃-BaTiO₃-K_{0.5}Na_{0.5}NbO₃.

 I. Structure and room temperature properties, J. Appl. Phys. 103 (2008) 034107.
- [37] D. Seol, H. Taniguchi, J.Y. Hwang, M. Itoh, H. Shin, S.W. Kim, Y. Kim, Strong anisotropy of ferroelectricity in lead-free bismuth silicate, Nanoscale. 7 (2015) 11561–11565.
- [38] Y. Saito, H. Takao, T. Tani, T. Nonoyama, K. Takatori, T. Homma, T. Nagaya, M. Nakamura, Lead-free piezoceramics, Nature. 432 (2004) 84–87.
- [39] D. Alikin, A. Turygin, A. Kholkin, V. Shur, Ferroelectric Domain Structure and Local Piezoelectric Properties of Lead-Free (Ka_{0.5}Na_{0.5})NbO₃ and BiFeO₃-Based Piezoelectric Ceramics, Materials (Basel). 10 (2017) 47.

- [40] N. Dong, X. Gao, F. Xia, H. Liu, H. Hao, S. Zhang, Dielectric and Piezoelectric Properties of Textured Lead-Free Na_{0.5}Bi_{0.5}TiO₃-Based Ceramics, Crystals. 9 (2019) 206.
- [41] J.Y. Li, R.C. Rogan, E. Üstündag, K. Bhattacharya, Domain switching in polycrystalline ferroelectric ceramics, Nat. Mater. 4 (2005) 776–781.
- [42] J. Abe, M. Kobune, T. Nishimura, T. Yazaw, Y. Nakai, Effects of manganese addition on pyroelectric properties of (Bi_{0.5}Na_{0.5}TiO₃)0.94(BaTiO₃)0.06 ceramics, Integr. Ferroelectr. 80 (2006) 87–95.
- [43] S. Patel, A. Chauhan, R. Vaish, Large pyroelectric figure of merits for Sr-modified Ba_{0.85}Ca_{0.15}Zr_{0.1}Ti_{0.9}O₃ ceramics, Solid State Sci. 52 (2016) 10–18.
- [44] M. Shen, W. Li, M.Y. Li, H. Liu, J. Xu, S. Qiu, G. Zhang, Z. Lu, H. Li, S. Jiang, High room-temperature pyroelectric property in lead-free BNT-BZT ferroelectric ceramics for thermal energy harvesting, J. Eur. Ceram. Soc. 39 (2019) 1810–1818.
- [45] S.T. Lau, C.H. Cheng, S.H. Choy, D.M. Lin, K.W. Kwok, H.L.W. Chan, Lead-free ceramics for pyroelectric applications, J. Appl. Phys. 103 (2008) 104105.
- [46] R. W. Whatmore, F.W. Ainger, Pyroelectric Ceramic Materials For Uncooled I.R. Detectors, in: J. Besson (Ed.), Adv. Infrared Sens. Technol., SPIE (1983) 261–266.